Effect of Friction Stir Welding on Dynamic Properties of AA2024-T3 and AA7075-T7351

Dynamic compressive flow behavior and its relation to yield stress and strain hardening were investigated

BY Y. J. CHAO, Y. WANG AND K. W. MILLER

ABSTRACT. A split Hopkinson pressure bar or Kolsky bar system was used to determine the dynamic compressive flow behavior of two materials. Dynamic, compressive stress-strain curves were obtained of AA2024-T3 and AA7075-T7351 aluminum alloys and their welds as produced by the friction stir welding process. To show the strain rate effect, quasistatic tests of these materials were also performed using a specimen configuration identical to that used in the dynamic tests. The experimental results showed 1) friction stir welding reduces the yield stress of the weld metal to below that of the base metal; 2) both materials exhibit the strain rate effect, *i.e.*, the yield stress is higher under higher strain rates; and 3) the strain hardening appears to be similar for various strain rates.

Introduction

Friction stir welding (FSW) is a relatively new technique for joining aluminum alloys (Ref. 1). Compared to traditional fusion welding, friction stir welding is a solid-state joining process that does not melt the materials and has the potential to avoid significant changes in microstructure and mechanical properties. The FSW process provides a method for joining some aluminum alloys that are not normally weldable. For example, AA2024 and AA7075 are not recommended for arc welding, but the friction stir welding process can be used to join these alloys without difficulty (Ref. 2).

Microstructure variation from the FSW process, as well as the development of the FSW process itself, has drawn much attention in past years (Refs. 3–10). However, the ultimate use of the weld is in structural application, which often involves the static, fatigue, dynamic or impact type loading found in automotive and aerospace applications. Weld strength, fracture and fatigue must be studied as well to ensure a safe and reliable operation of the welded structure. Recent studies along this direction include Refs. 11–13.

In many applications, the welded structure may be subjected to dynamic load such as impact and explosion. It is, therefore, important to understand the mechanical properties of structural materials at the high strain rate to which the components may be subjected during service. The objective of the current work is to evaluate changes in the compressive mechanical properties due to the friction stir welding process. Aluminum alloys AA2024-T3 and AA7075-T7351 were studied. Samples were tested at a quasistatic rate using a standard hydraulic load frame and at high strain rates using a split Hopkinson pressure bar system. Results are reported in the form of stress-strain curves for different strain rates. Hardness values of the material before and after testing are also presented. The results can be used in evaluating the dynamic response of the FSW structures as well as in studying the material flow behavior of the friction stir welding process.

KEY WORDS

Friction Stir Welding
Hopkinson Bar
Strain Rate Effect
Aluminum Alloys
Solid-State Welding
Strain Hardening

Y. J. CHAO, Y. WANG and K. W. MILLER are Professor and Research Associates, respectively, with the Department of Mechanical Engineering, University of South Carolina, Columbia, S.C.

Experiment

Dynamic Tests

The split Hopkinson pressure bar (SHPB) technique (Refs. 14–17) is one of the most popular experimental techniques for studying dynamic behavior of materials under high strain rate loading. The principle of this experimental technique is based on the well-known one-dimensional theory of wave propagation in elastic bars and the interaction between a stress pulse and a short cylindrical specimen, which is sandwiched between the input and output bars. A schematic illustration of the SHPB in this study is shown in Fig. 1.

The typical SHPB setup consists of a gas gun, a striker, an input bar and an output bar. A gas gun accelerates the striker bar (projectile). The resulting impact with the input bar produces an elastic, compressive pulse (incident pulse ε_i). The elastic compressive pulse propagates down the input bar until it reaches the input bar/specimen interface. This compressive pulse then partially reflects back into the input bar (reflected pulse ε_r) and partially transmits through the specimen into the output bar (transmitted pulse ε_t). These three stress pulses in the bars are recorded by strain gauges on the input and output bars. The amplitude of the incident pulse depends on the striker velocity. In addition, the length of the incident pulse is twice the time needed for an elastic stress pulse to travel the length of the striker bar.

Based on one-dimensional stress wave theory, the values of stress and strain in the specimen can be determined

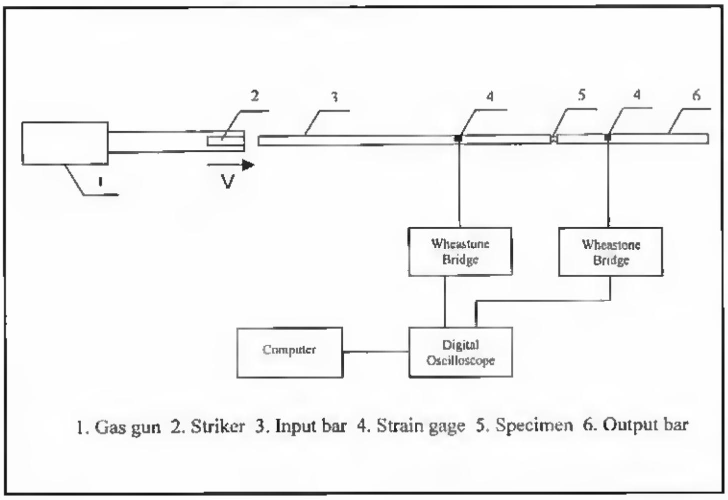

Fig. 1 — Schematic diagram of the split Hopkinson pressure bar.

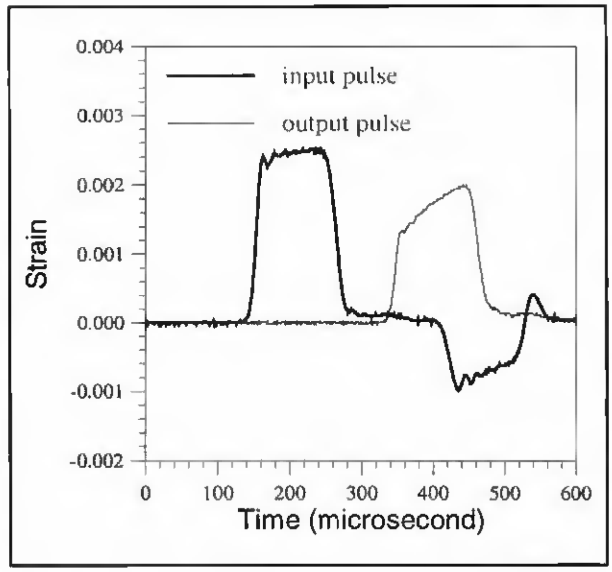

Fig. 2 — Typical incident, reflected and transmitted pulses from a split Hopkinson pressure bar test.

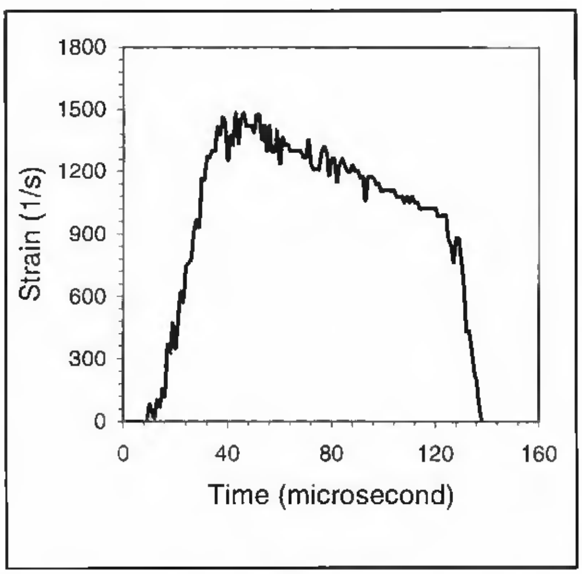

Fig. 3 — Typical strain rate variation from a split Hopkinson pressure bar test.

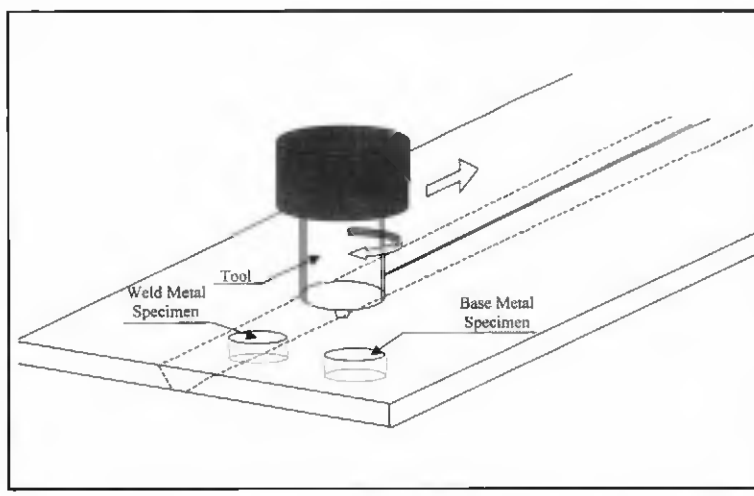

Fig. 4 — Schematic of the friction stir welding process and specimen locations.

by using records of strain gauges located on the input/output bars. The axial stress $\sigma_s(t)$, strain $\varepsilon_s(t)$, and strain $\dot{\varepsilon}_s(t)$ rate in the specimen can be calculated as follows (Ref. 17):

$$\sigma_s(t)=\frac{EA}{2A_s}\left[\varepsilon_i(t)+\varepsilon_r(t)+\varepsilon_t(t)\right] \quad (1)$$

$$\varepsilon_s(t)=\frac{C_0}{L_s}\int_0\left[\varepsilon_i(t)-\varepsilon_r(t)-\varepsilon_t(t)\right]d\xi \quad (2)$$

$$\dot{\varepsilon}_s(t)=\frac{C_0}{L_s}\left[\varepsilon_i(t)-\varepsilon_r(t)-\varepsilon_t(t)\right] \quad (3)$$

Where t = time; A = cross-sectional area of the bar; E = Young's modulus of the bars; C_0 = speed of the elastic longitudinal wave in the bar; L_s = thickness of the specimen; A_s = cross-sectional area of the specimen; $\varepsilon_i(t)$, $\varepsilon_r(t)$, = incident and reflected axial strain signals recorded by strain gauge on the input bar as a function of time t; and $\varepsilon_t(t)$ = transmitted axial strain signal recorded by strain gauge on the output bar as a function of time t.

Therefore, the constitutive relationship of the specimen material at a certain strain rate can be obtained using Equation 1.

A SHPB system was designed and built by the mechanics group in the Department of Mechanical Engineering, University of South Carolina. The steel input and output bars had lengths of 2.4 m (94.5 in.) and 1.2 m (47.2 in.), respectively. They were instrumented with semiconductor strain gauges at two locations. At each location, two gauges were oriented axially and were bonded to the opposite sides of the bar to cancel any bending disturbance. The striker bar and input/output bars had the same diameter 25.4 mm (1.0 in.) and were made of O1 tool steel. The speed of the elastic longitudinal wave of these steel bars was 5000 m/s (16,404 ft/s).

Typical recorded signals from the strain gauges are shown in Fig. 2. The incident pulses were generated using a 287-mm (11.3-in.) striker bar with approximately 10 m/s (32.8 ft/s) impact speed. Different strain rate tests can be performed by using different length striker bars and generating different impact velocities. The strain rate variation from a typical test is shown in Fig. 3. The average strain rate for this test of 1200/s is only an

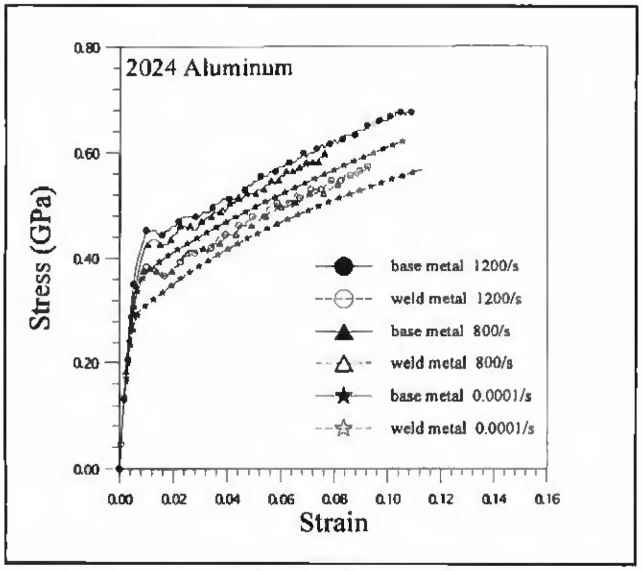

Fig. 5 — Stress-strain curves for AA2024-T3 at three strain rates.

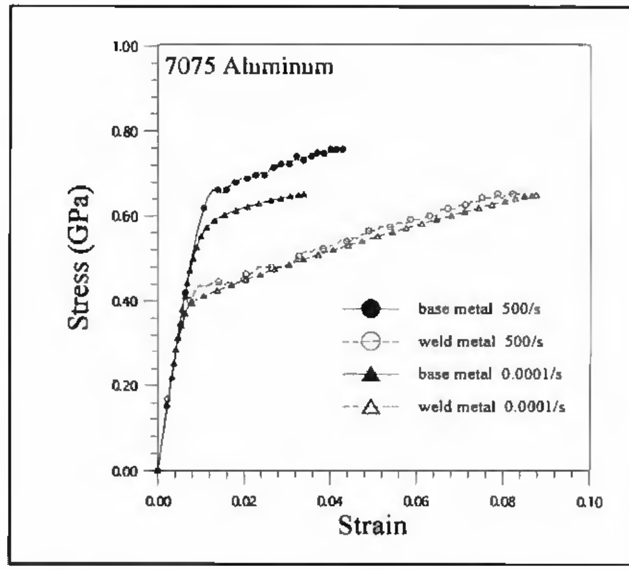

Fig. 6 — Stress-strain curves for AA7075-T7351 at two strain rates.

"eyeball estimate" because strain rate is not constant in this type of SHPB test.

Specimens

The alloys selected were AA2024-T3 and AA7075-T7351. Two 9.5-mm- (0.374-in.-) thick plates for each type of the material were joined using friction stir welding on the Supermill-5VR mill at the University of South Carolina. The FSW tool is made of tool steel with a threaded pin. The outside diameter of the tool is 28 mm (1.1 in.) and the pin diameter and length are 10 mm and 7.5 mm (0.394 and 0.295 in.), respectively. The travel speed for welding is 113 mm/min (4.4 in./min) with a spindle speed of 215 rpm. A schematic of the friction stir welding process is shown in Fig. 4.

After welding, cylindrical specimens were cut from the base metal and the weld zones of the aluminum plate. The orientation of the cylindrical axis of the specimen was perpendicular to the aluminum plate, as shown schematically in Fig. 4. The specimen has a diameter of 20 mm (0.787 in.) and thickness of 9 mm (0.354 in).

Quasistatic Test

To evaluate strain-rate sensitivity, quasistatic compression tests were run on an MTS hydraulic load frame. A fixture was made for the compression tests, which were conducted with a crosshead velocity producing a constant strain rate of 0.0001/s. Identical specimen configurations were used in both the dynamic and the quasistatic tests, allowing for a much more reliable comparison of data at various strain rates.

Microhardness Tests

To examine local variations in the mechanical properties that occur in and around the friction stir weld zone, the hardness of the welding zone was tested with a Micromet microhardness tester. A Knoop indentor was used with a load of 200 g and dwell of 15 s. The Knoop hardness was measured across the centerline of the welded plate.

All compression tests and hardness tests were performed at room temperature, approximately 22°C.

Table 1 — Yield Stress of Different Materials at Different Strain Rates

	Strain Rate (1/s)	Yield Stress $\sigma_{0.2}$ (GPa)
AA2024-T3 base metal	1200/800/0.0001	0.420/0.381/0.335
AA2024-T3 weld metal	1200/800/0.0001	0.352/0.346/0.290
AA7075-T7351 base metal	500/0.0001	0.627/0.554
AA7075-T7351 weld metal	500/0.0001	0.414/0.398

Results and Discussion

The dynamic tests were performed at strain rates of 800/s and 1200/s for AA2024-T3 and 500/s for AA7075-T7351. The experimentally determined compressive stress-strain relations at different rates are shown in Figs. 5 and 6, respectively, for AA2024-T3 and AA7075-T7351. The comparison of the yield stress determined at 0.2% offset for different rates is listed in Table 1. Also, the yield stress at various strain rates are plotted vs. strain rate in log scale in Fig. 7.

It can be seen from Figs. 5 and 7 and Table 1 that both the AA2024-T3 base metal and the friction stir weld show an increase in yield stress with strain rate. Compared to quasistatic loading, the yield stresses for the base metal and weld metal at 800/s increased 14% and 19%, respectively. From 800/s to 1200/s, the yield stress for the base metal increased by 10%. However, the strain-rate sensitivity for weld metal is not as pronounced from 800/s to 1200/s. Under 1200/s dynamic loading, the yield stress of the weld metal is 16% less than that of the base metal, and it is about 13% less in yield stress under quasistatic loading.

The strain hardening after yielding for both the base and FSW materials appear to be very similar. It may be concluded the effect of the FSW process on the mechanical property of AA2024-T3 under both dynamic and quasistatic loading was approximately identical, *i.e.*, reducing the yielding stress by about 13% to 16% without changing the hardening behavior. This similarity in hardening could be due to the base metal of AA 2024-T3

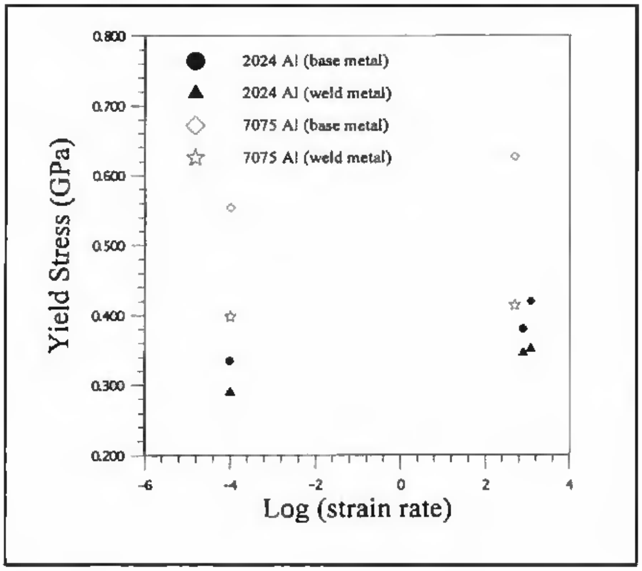

Fig. 7 — Yield stresses vs. strain rate (log scale).

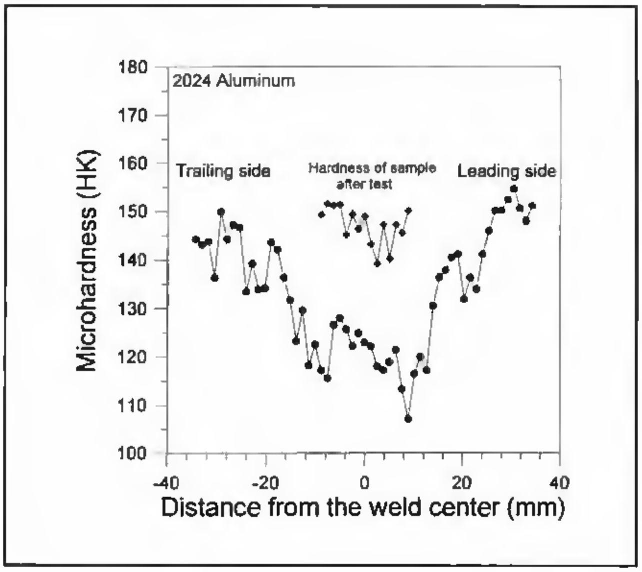

Fig. 8 — Knoop hardness for welded AA2024-T3.

being stretched and naturally aged to stable conditions. The FSW process relieved the stretch and eliminated the work hardening; consequently, parallel shift of the curves is seen in Fig. 5.

For AA7075-T7351, an increase in yield stress of 13% from a strain rate of 0.0001/s to 500/s was found, as shown in Figs. 6 and 7 and Table 1. However, the yield stresses for weld material at quasi-static and dynamic loading rates are almost identical, which means there is no apparent rate sensitivity up to 500/s in compression. Similar to AA2024-T3, the yield stresses for weld metal decrease at both high-rate and quasistatic loading compared to those of the base metal. Furthermore, the degree of decrease through friction stir welding at 500/s was higher than at 0.0001/s, as seen in Fig. 7. The strain-hardening behavior of both the base metal and the weld metal appears to be very similar, *i.e.*, seen as a parallel increase as the strain rate is increased.

It should be mentioned the specimen (20 mm diameter and 9 mm thick) contains different microstructure regions generated by the friction stir process. Therefore, data presented here are "lumped" material properties prototypical for the weld as a whole, not for the individual microstructure.

The Knoop microhardness as a function of distance from the centerline of the friction stir weld for AA2024-T3 and AA7075-T7351 is shown in Figs. 8 and 9, respectively. Three regions are obvious from the hardness distribution in Figs. 8 and 9: 1) the central part of the weld corresponds to the fully plasticized region of the FSW weld; 2) the heat-affected zone has the lowest hardness; and 3) the base metal has the highest hardness. The variation of the hardness from base metal to weld metal is larger for AA7075-T7351 than AA2024-T3, which correlates with the yield stress results shown in Fig. 7. The base metal on two sides of the FSW weld show a slight difference in hardness, possibly due to the asymmetric nature of the process (trailing vs. leading side).

The hardness of the samples (AA2024-T3 weld metal at 1200/s; AA7075-T7351 weld metal at 500/s) used in the dynamic test was also measured after the tests. As shown in Figs. 8 and 9, dynamic loading increased the hardness of the weld and, accordingly, the yield stress. This is obviously due to the work hardening of the material, which has had a large permanent plastic strain.

Note the tests were performed approximately two months after the FSW was made. This time is probably sufficient for AA2024-T3 to stabilize, but this is not true for AA7075-T7351. Both the base metal and the weld are expected to age continuously for AA7075-T7351; thus, higher strength may be obtained later.

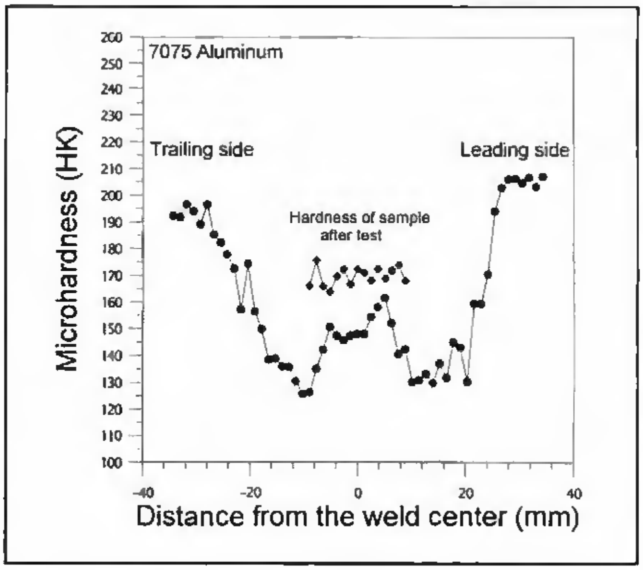

Fig. 9 — Knoop hardness for welded AA7075-T7351.

Conclusions

A split Hopkinson pressure bar or Kolsky bar system typically used to determine the dynamic behavior of materials was introduced. Dynamic, compressive stress-strain curves were obtained for AA2024-T3 and AA7075-T7351 aluminum alloys, as well as their weld material produced by the FSW process. The experimental results indicated the following:

1) Yield stresses of both base and friction stir weld material of AA2024-T3 exhibited rate sensitivity. In addition, AA7075-T7351 base metal had some

rate dependence. However, no rate effect was found for AA7075-T7351 friction stir weld material up to the strain rate of 500/s.

2) Friction stir welding reduced the yield stress of both AA2024-T3 and AA7075-T7351 under both high strain-rate and quasistatic loading conditions.

3) Strain hardening is similar for both materials at various strain rates.

The results reported in the current paper can have two applications. One is to aid in process modeling – *e.g.*, material flow characterization. Recent studies at the University of South Carolina (Ref. 18) indicate the strain rate near the vicinity of the tool pin can be as high as 1000 1/s. The results in this paper provide preliminary technical information for such a modeling effort. It is, however, understood high material strain rate occurs at elevated temperature during welding. Therefore, our future work will study material rate data, similar to that reported here but at high temperatures for friction stir welding process modeling.

The immediate and second application of the results reported in this paper are for structural performance, *e.g.*, load-carrying capability, fracture and reliability of the weld. As mentioned in the introduction section, welded structures may be subjected to dynamic impact load. As such, high strain (loading) rate behavior of the weld, such as the data reported here, is essential in modeling and understanding the dynamic response of the welded structures.

Acknowledgments

The authors are grateful for laboratory assistance from Daniel Wilhelm of the University of South Carolina. Funding from the National Science Foundation through NSF/EPSCoR cooperative agreement #EPS-9630167 and the Air Force Research Lab/Materials Lab (AFRL/ML), with Dr. Kumar Jata, is greatly appreciated.

References

1. Dawes, C. T., and Thomas, W. M. 1996. Friction stir process welds aluminum alloys: a new friction welding technique allows easy welding of normally difficult-to-join materials. *Welding Journal* 75(3): 41.

2. *ASM Handbook, Vol. 6.* 1983. ASM International, Materials Park, Ohio, pp. 373.

3. Rhodes, C. G. 1997. Effects of friction stir welding on microstructure of 7075 aluminum. *Scripta Materialia* 36(1): 69–75.

4. Flores, O. V., Kennedy, C., Murr, L. E., Brown, D., Pappu, S., Nowak, B. M., and McClure, J. C. 1998. Microstructural issues in a friction-stir-welded aluminum alloy. *Scripta Materialia* 38(5): 703–708.

5. Frigaard, G., and Midling, O. T. 2001. A process model for friction stir welding of age hardening aluminum alloys. *Metallurgical and Materials Transactions* A 32A(5): 1189–1200.

6. Mahoney, M. W., Rhodes, C. G., Flintoff, J. G., Spurling, R. A., and Bingel, W. H. 1998. Properties of friction-stir-welded 7075 T651 aluminum. *Metallurgical and Materials Transactions* A 29A(7): 1955–1964.

7. Rhodes, C. G., Mahoney, M. W., Bingel, W. H., Spurling, R. A., and Bampton, C. C. 1997. Effects of friction stir welding on microstructure of 7075 aluminum. *Scripta Materialia* 36(1): 69–75.

8. Benavides, S., Li, Y., Murr, L. E., Brown, D., and McClure, J. C., 1999. Low-temperature friction stir welding of 2024 aluminum. *Scripta Materialia* 41(8): 809–815.

9. Li, Y., Murr, L. E., and McClure, J. C. 1999. Flow visualization and residual microstructures associated with the friction stir welding of 2024 aluminum to 6061 aluminum. *Materials Science and Engineering* A 271(1-2): 213-223.

10. Chao, Y. J., Qi, X. H. 1999. Thermal and thermo-mechanical modeling of friction stir welding of aluminum alloy 6061-T6. *Journal of Material Processing and Manufacturing* 7(2): 215–233.

11. Jata, K. V., Sankaran, K. K., and Ruschau, J. J. 2000. Friction stir welding effects on microstructure and fatigue of aluminum Alloy 7050-T7451. *Metallurgical and Materials Transactions* A 31A(9): 2181–2192.

12. Hu, W. S., Meletis, E. I. 2000. Corrosion and environment-assisted cracking behavior of friction stir welded Al 2195 and Al 2219 alloys. *Material Science Forum*, pp. 331-333: 1683-1688, Part 1–3.

13. Haagensen, P. J., Midling, O, T. and Ranes, M. 1996. Fatigue performance of friction stir butt welds in a 6000 series aluminum alloy. *International Journal of Fatigue* 18(7): 508.

14. Kolsky, H. 1949. An investigation of the mechanical properties of materials at very high rates of loading. *Proc. Phys. Soc.* (London) B62: 676–700.

15. Lindholm, U. S. 1964. Some experiments with the Split Hopkinson Pressure Bar. *J. Mech. Phys. Solids* 2: 317–335.

16. Nicholas, T. 1992. *Impact Dynamics*, eds. Zukas, J. A., Nicholas, T., Swift, H. L., Greszczuk, L. B., and Curran, D. R. Krieger, Malabar, Fla.

17. *ASM Handbook.* 1985. High strain rate testing. ASM International, Materials Park, Ohio, 8:198.

18. Private communication with Professor Anthony P. Reynolds, University of South Carolina, 2001.